

Effect of impact-generated shock wave in a nozzle on the multiple pulse jet formation

Anirut Matthujak^{1*}, Kulachate Pianthong¹, Mingyu Sun² and Kazuyoshi Takayama²

¹ Department of Mechanical Engineering, Faculty of Engineering, Ubon Ratchathani University,
Ubon Ratchathani, 34190, Thailand,

Tel: +66-45-353380, Fax: +66-45-353333, *Email: Anirut.Mat@gmail.com, A.Matthujak@ubu.ac.th

² Interdisciplinary Shock Wave Research Laboratory, Institute of Fluid Science, Tohoku University,
Sendai, 980-8577, Japan,
Tel: +81-22-2175285 ext 5286

Abstract

We reported the multiple pulse jet formation of high-speed liquid jet generated by impact acceleration method. However, the cause of the multiple pulse jet generation and wave interaction inside a nozzle are not yet experimentally resolved. In this paper we discuss the propagation and reflection of shock waves inside a nozzle and their contribution to the multiple pulse jet formation. To clarify the multiple pulse jet formation, we used a 10.6 mm x 10.6 mm container of water with thick acrylic observation windows and quantitatively visualized waves by using double exposure holographic interferometry and inserted an optical fiber pressure transducer of 0.1 mm in diameter and resonant frequency of 100 MHz into the 0.7 mm diameter nozzle exit hole for the pressure measurement after a projectile at 300 m/s impacted the liquid surface in the nozzle. The pressure behind the shock wave in liquid was 1.24 GPa generated by the projectile impact and successive over-pressures caused by the released wave from longitudinal and transversal waves in the nozzle metal wall and multiple reflections of waves in the liquid were accurately measured. Moreover, negative pressures detected with the optical fiber pressure transducer are attributable to impact flash and have no physical significance. Comparing visualization of high-speed liquid jet, pressure measurements, holographic interferometric visualization and one-dimensional analysis, we conclude the multiple reflections in nozzle liquid caused multiple impulsive acceleration of high-speed jet and the contribution of stress waves in nozzle metal to liquid jet formation is not significant.

Keywords: High-speed liquid jet, Impact acceleration method, Pressure measurement, Shock wave

1. Introduction

In 1958, Bowden and Brunton [1, 2] invented impact acceleration technique. It is today widely adopted by many researchers for generating high-speed liquid jets [3-

11]. However, despite of its practical successes, the dynamic process of high-speed jet formations has been not yet well analyzed. Upon high-speed projectile impingements, some numerical and analytical studies were reported regarding the high-pressure generations in the container and hence resulting jet formations through a nozzle. However, due to inherent complexities, pressures or pressure waves in the container of liquid have not been resolved yet. Typical results of facility developments and flow analyses were well documented by O'Keefe et al. [12] in 1967, Ryhming [13] in 1973, and Glenn [14] in 1975.

In 1995, Lesser [15] derived basic equations, analyzed the supersonic jet generation by assuming propagation of acoustic waves, and compared liquid jet generation with experiments obtained by a Bowden-Brunton device. Although he took wave reflection into consideration, details of shock wave interactions occurring in the nozzle were not considered.

In 2003, Pianthong et al. [16] analyzed, by using a one-dimensional analytical model, the presence of simple, strong shock waves and their multiple reflection in a container of liquid. To interpret intermittent formations of jets, by drawing a wave diagram they explained the motion of incident, reflected, and transmitted shock waves were and succeeded to compare their analytical results with experimental observations [6, 8, 10, 11, 15]. They estimated time variations of pressures in the container of liquid and eventually jet speeds.

In 2005, Milton et al. [17] numerically simulated supersonic liquid jet formations by using the Autodyne 2-D and clarified shock wave motions in a rigid container of liquid impacted by a projectile and intermittent jet generation.

All of the previous studies, the containers of liquid are assumed to be rigid body and hence the generation and propagation of stress wave acceleration method can be totally neglected. We, however, realized that in real metal container it deformed by high-speed impacts and hence

the presence of longitudinal and transversal waves possibly created in metallic parts of the container would affect the jet formation. So far as in our literature survey, the contribution of stress waves in metal walls to the wave interactions inside the metal container have never been taken into account. To clarify the contribution of these waves in metal and their released waves into water, we manufactured a 10.6 mm x 10.6 mm cross sectional container of water and visualized, by using double exposure holographic interferometry, impact generated inherent shock waves in water and also shock waves converted from stress waves.

Aiming to conduct precise pressure measurements, we inserted a 0.1 mm diameter optical fiber probe pressure transducer of 100 MHz resonant frequency into a 0.7 mm diameter nozzle hole. This pressure transducer is unique not only for its compact geometry but also due to its working principle, that is, pressure variations are detected in terms of refractive index variation corresponding to density change in water.

This device is completely free from any electric noises. However, in measuring impact phenomena, the pressure transducer negative pressure values never agreed with physical interpretations. Then an effort was made to experimentally interpret such puzzling responses and then we eventually revealed that these false signals were attributable to the optical responses of the optical fiber pressure transducer to the impact flash caused at high-speed projectile impingement and somehow transmitted into the optical fiber. Moreover, results of the one-dimension analysis of shock reflection inside a nozzle is used to help in description and to compare with the experiment results of the pressure measurement and the high-speed liquid jet visualization for clearly understanding the phenomena occurred inside the nozzle during high-speed liquid jet generation.

2. Experimental facility

We used an impact driven method for high-speed liquid jet generation [1, 2]. The liquid contained in the nozzle cavity is impacted by a high speed projectile. The high speed projectile needed in this technique is produced by the vertical two stage light gas gun (VTSLGG), shown in Fig 1.

The component detail and the operation procedure of the VTSLGG have been described [18, 19]. Note that the impact velocity (V_p) of 300 m/s, the conical nozzle and water is used for high-speed liquid jet generation in this experiment.

3. Pressure measurement system

A 0.1 mm diameter optical fiber pressure transducer (FOPH2000 RP Acoustics Co.Ltd.) we used is one of the most sophisticated pressure transducers commercially available. We inserted it into a 0.7 mm diameter nozzle hole as shown in Fig. 2. Being so thin, it was supported by a jig and placed in the center of the nozzle hole so as to hold exactly parallel to the nozzle axis. Its plastic shroud was removed and glued in the jig as shown in Fig. 3.

A projectile ejected from the muzzle has a precursory blast wave, which arrives at the liquid surface before the projectile impacts and may disturb the surface. As the test gas is atmospheric air and the projectile speed is close to sonic speed or even faster, the blast wave speed exceeds well over 700 m/s, which results in over-pressure ranging 300 to 400 kPa. Since such a high pressure wave disturbs the liquid surface, to get rid of the disturbance, we attached a blast relief section at the muzzle. It consists of a blast relief chamber to accommodate a blast wave and a launch tube having 8 mm diameter holes in 3 rows, through which the blast wave discharged and spontaneously attenuating to sonic waves as shown in Fig. 2.

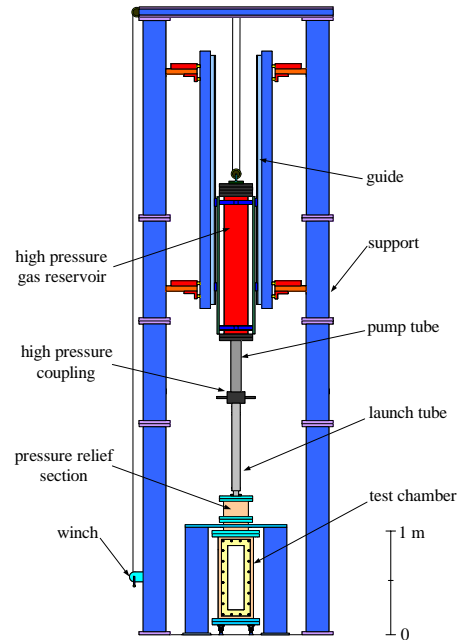


Figure 1. Vertical two-stage light gas gun (VTSLGG)

The output signal from optical fiber pressure transducer was detected by a photo-detector and stored in a digital oscilloscope. The principle of the optical fiber pressure transducer is as following: The pressure variation and hence density variation would vary the refractive index in water. Source laser beam transmitted through an optical fiber illuminates a very small spot at which pressure varies and simultaneously reflected light from the spot at which refractive index variation modulates the reflected light signal. The modulated light signal is transmitted and recorded by a photo-detector.

Then the interference between the event modulated light signals and reference signals from the source light is accurately recorded by a photo-detector. As the source laser beam is monochromatic and coherent so that the temporal variation of pressures at a spot of 0.1 mm diameter can be detected at a high frequency response of 100 MHz by employing a reliable equation of state of water. Further information of the optic fiber pressure transducer is found in [20, 21]. Its tip is positioned exactly at 4 mm from the bottom of the nozzle. The schematic diagram of its setting is shown in Fig. 3.

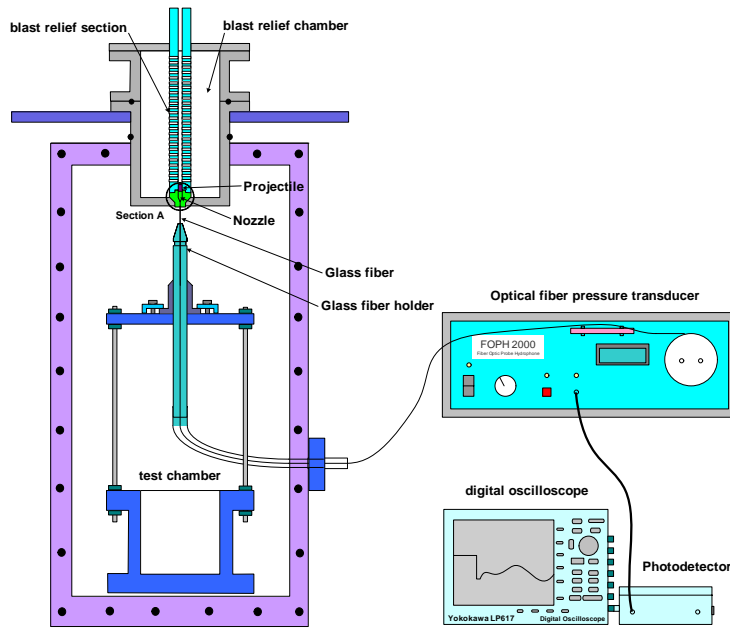


Figure 2. Pressure measurement system

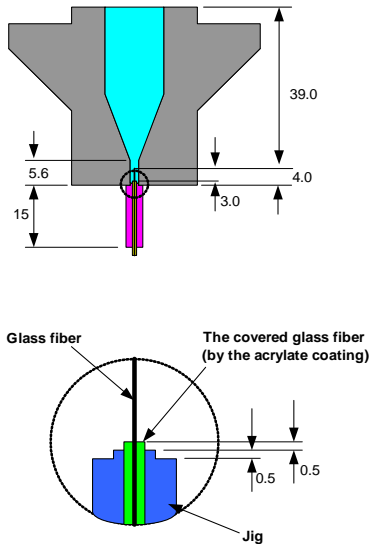


Figure 3. Optical fiber pressure transducer setting

4. Pressure history

A result of pressure measurements is shown in Fig. 4. However, we observed very high negative pressures in the nozzle hole at the moment of the projectile impact. Such a negative pressure is hardly to physically understand. It was reported that in a vertical shock tube filled with bubbly Freon, negative pressures were detected in front of incident shock wave by using a pressure transducer imbedded in the shock tube metal wall just before the arrival of main shock wave. The negative pressure was not caused by metal wall deformation. Presumably it was caused by the fact that pressures in the metal wall became locally negative when

a longitudinal wave precursory to the incident shock in liquid [22]. From the preliminary test, however, the negative pressures so far we observed in the present experiment are attributable to impact flash and have no physical significance.

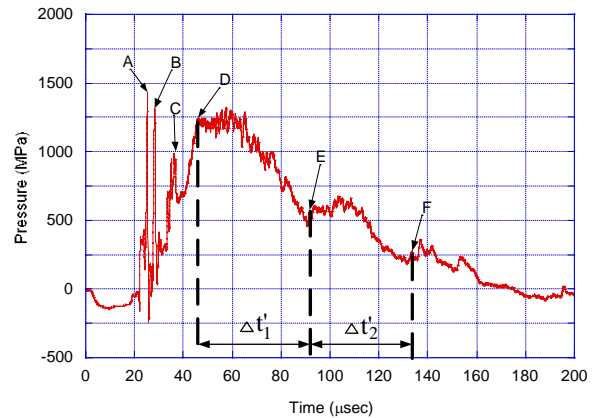


Figure 4. Shadowgraph optical setup for high-speed video recording

We observe the pressure fluctuation and the presence of three peak over-pressures, marked as A, B and C. These peak pressures A, B, and C correspond to the shock waves originated from longitudinal and transversal waves initially propagating in the container metal wall and spontaneously released into water and the incident shock wave in water, respectively. Then, the following three peak over-pressures marked at points D, E and F

correspond to 1.24, 0.602 and 0.273 GPa, respectively, which indicate multiple reflections of the shock wave C. The time intervals of peak pressures between D and E (Δt_1) and between E and F (Δt_2) are 45.08 and 38.82 μ s, respectively. From the visualization in Fig. 5 and from [23], time intervals (Δt_1) between 1st and 2nd jet tips and (Δt_2) between 2nd and 3rd jet tips are 24 and 32 μ s, respectively.

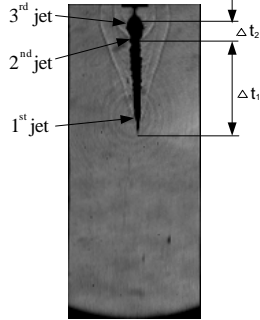


Figure 5. Intermittent water jet acceleration (from [23])

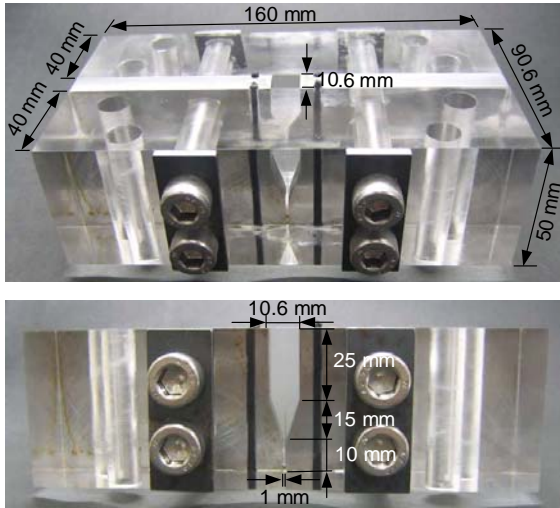


Figure 6. A 10.6 mm x 10.6 mm square cross sectional nozzle, notice very thick acrylic wall thickness

Peak pressures at D, E and F represent multiple reflections in liquid, which drive corresponding jets at time intervals of Δt_1 and Δt_2 . Due to the insertion of the jig from the nozzle exit hole, pressures increases inside the nozzle take longer holding time and resulting higher pressures destroyed the jig which was tightly glued in the nozzle hole. However, as later see in holographic interferometric visualization, a Mylar diaphragm of 50 μ m in thickness attached at the nozzle exit hole was much weaker than the jig holder. Moreover, in visualization we see that peak pressure marked D in Fig. 4 drives the first jet and quickly decays after reaching the maximum pressure. The pressure decrease corresponds to the rupture of the plastic diaphragm at the nozzle exit. The time intervals of pressure peaks in pressure measurements are longer than that in visualization. Even though the values of pressure peaks A and B are relatively high, their

time integrations, that are impulse, are not as large as those corresponding D and E. The contribution of the first two peaks A and B to the first jet formation is much smaller.

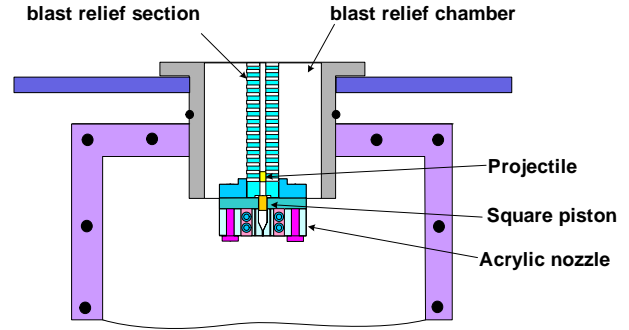


Figure 7. A square cross sectional nozzle arrangement

5. Precursory released stress waves in water

We visualized, by using double exposure holographic interferometry, the wave motion in the square container (as shown in Fig. 6) after piston impingement. Note the square cross sectional nozzle setting at the tip of blast relief section is shown in Fig. 7. Time markers are attached on these sequential interferograms. Although the experiments were repeatable, the time marker and the corresponding wave position slightly scattered within a few $\pm \mu$ s. Selective sequential holographic interferograms are shown at $V_p = 374 \pm 4$ m/s are presented in Figs. 4.13a-h: (a) 8 μ s; (b) 15 μ s; (c) 21 μ s; (d) 32 μ s; (e) 64 μ s; (f) 80 μ s; (g) 90 μ s; and (h) 114 μ s.

At 8 μ s after the impingement, in Fig. 8a, longitudinal and transversal waves in the metal wall and acrylic windows are spontaneously released into water and formed oblique shock waves. As longitudinal and transversal wave speeds in the steel wall are 5.9 km/s and 3.2 km/s, respectively, and those in acrylic are 2.7 km/s and 1.4 km/s, respectively, and much faster than the sound speed in water. The inclination angle of these oblique shock waves θ is expressed by $a_{\text{water}}/a_{\text{solid}} = \sin\theta$ where a_{water} and a_{solid} are sound speeds in water and solid, respectively. An oblique shock wave L observable in Fig. 8a is a released longitudinal wave and is inclined about 15°, whereas one defined by this relationship is about 28°. The experimental inclination angle (26.5°) is closer to one defined for the oblique shock wave into water corresponding to the transversal wave marked as T.

Fringes distributed normal to the solid wall correspond to the shock wave LA released from the longitudinal wave in acrylic, which nearly merge with the released transversal wave T from metal wall. At the spot where the normal shock and oblique shock intersect, the oblique shock changes of its inclination angle of 5°, which implies the merger of T and LA. The second normal shock corresponds to shock wave in water S, which were formed by piston compression. It should be noticed that fringes observable in front of L are caused by temperature fluctuations

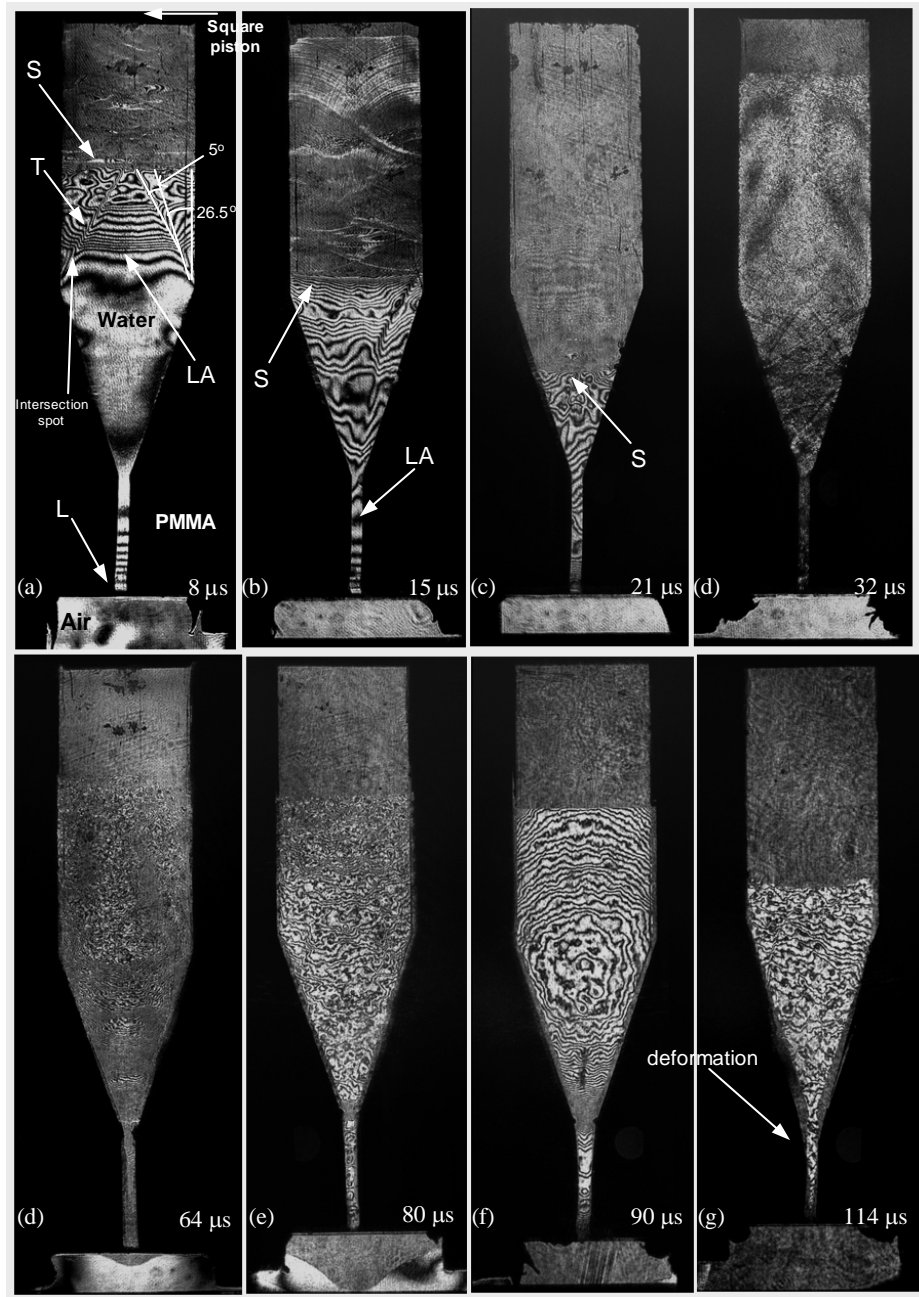


Figure 8. Sequential holographic interferograms of precursory stress waves in metallic side wall and shock waves released in water, $V_p = 362$ m/s at the elapsed time of : (a) $8 \mu\text{s}$; (b) $15 \mu\text{s}$; (c) $21 \mu\text{s}$; (d) $32 \mu\text{s}$; (e) $64 \mu\text{s}$; (f) $80 \mu\text{s}$; (g) $90 \mu\text{s}$; and (h) $114 \mu\text{s}$. Notice main shock wave and precursory stress waves in the metal wall and acrylic windows.

L and T passing through the tapered parts of the nozzle reflected obliquely interacted two-dimensionally with each other. Released waves and S are still identified in Fig. 8b,c and moved into the nozzle part enhancing pressures. Container shapes are different between the present square cross sectional case and conical one in the pressure measurement in Fig. 4. The modes of impacts are different between the present case and that in Fig. 4. In the square cross sectional container, the projectile impacted on the square piston, whereas in the circular cross sectional

container in the pressure measurement, the projectile directly impacted the liquid surface. If one neglects all these differences and compares Fig. 8, for the sake of simplicity, with the pressure measurements in the nozzle hole as shown in Fig. 4, A and B marked in Fig. 4 correspond to L and T in Fig. 8, and C in Fig. 4 corresponds to S in Fig. 8.

The top part in Fig. 8d-g corresponds to D in Fig. 4, which consists of the assembly of wavelets and reflected shock waves, exhibiting a totally disturbed region. Despite of the difference of container

geometries and projectile impact modes in Fig. 4 and Fig. 8, the time variations of wave motion and pressures show many common features.

We put a Mylar diaphragm of 50 μm in thickness at the nozzle exit to hold liquid from the vertical nozzle hole. As seen in Fig. 8f-h, it did not rupture immediately after the high-pressure loading but started to gradually bulge and eventually ruptured at about 90 μs after the projectile impingement. At that time, the piston shown as dark area on the top started to move downward. With the jet initiation, the resulting nozzle flow thickens boundary layer displacement thickness and hence reduces water mass flow rate. Simultaneously, the metal wall deformation became visible as seen in Fig. 8h. With the initiation of nozzle flows, expansion waves propagate from the nozzle to the piston surface. Such multiple reflections of shock waves and expansion waves eventually accelerate intermittently liquid jets.

6. Comparison with one-dimensional analysis

To analytically interpret intermittent acceleration of liquid jets, we used a one-dimensional model of shock interactions inside a container of liquids [12-16]. Wave interactions inside the container and the contribution of stress waves to the jet formation were not discussed previously. In the previous section, we clarified the negligibly small contribution of precursory shock waves to jet formation. The result of the pressure measurement in Fig. 4 clearly indicated the presence of underwater shock wave and that released from stress waves in metal wall. However, as already discussed in the previous section, A, B, and C peaks merged together in the nozzle and drove the first jet tip. If a nozzle exit is not sealed by a diaphragm, peak pressures A and B may independently accelerate corresponding jets. However, their impulse is not so large that resulting jet formations may not be remarkable.

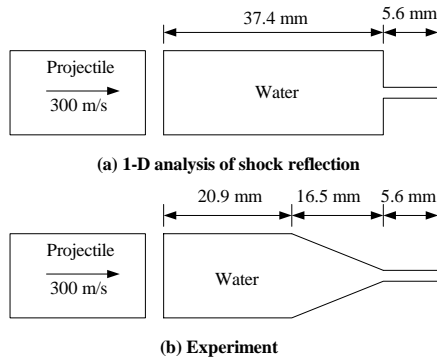


Figure 9. Diagram of inside nozzle geometry

In this experiment, the container shape has a long taper section and a long straight nozzle as shown in Fig. 9b but in the present analytical model, the tapered section portion was replaced with a straight end wall as shown in Fig. 9a. We applied analysis to this geometry

in the similar way as [16]. The result so far obtained agreed in part with the present experiment.

With the present step model, an x-t diagram of shock reflection, transmission and jet generation are drawn as shown in Fig. 10. The shock reflection, shock transmission, and particle velocity are presented in Table. 1. Pressures driving the individual 1st, 2nd and 3rd jets are 0.88, 1.74 and 2.3 GPa, respectively. The time intervals of Δt_1 and Δt_2 are 27.64 and 20.05 μs , respectively. Although the time interval of peak pressures and the jet formations are different between the pressure measurement and the present analyses, the identical wave motion is assumed. This implies that the difference of nozzle geometries affects significantly jet characteristics [11].

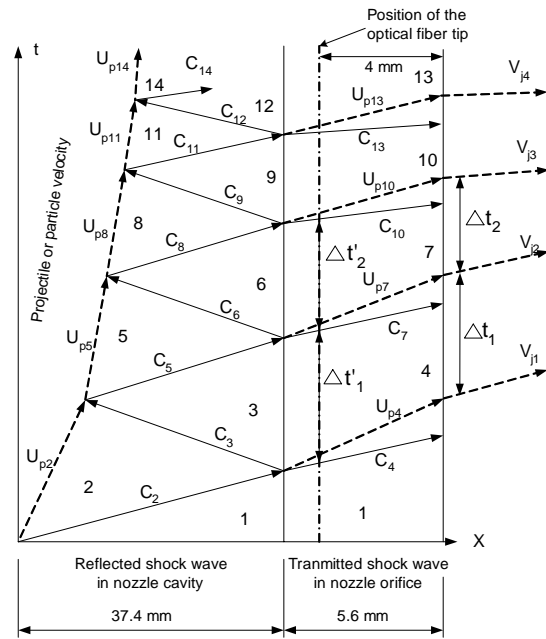


Figure 10. The x-t diagram of shock reflection, transmission and jet generation in a nozzle

Comparing the pressure measurement with the present analysis, we found that durations of time of pressure plateaus Δt_1 and Δt_2 in Fig. 4 correspond to the duration of time at which constant shock speeds are maintained in the regions of Δt_1 and Δt_2 in Fig. 10 and the time interval Δt_1 between the 1st and the 2nd jet tips and Δt_2 between the 2nd and the 3rd jet tips shown in Fig. 10 correspond to these in Fig. 5. The 1st jet speed, V_{j1} , in the present analysis corresponds to the visualization of the high-speed liquid fuel jet are compared in Table 2.

The one-dimensional analysis shows that 1st, 2nd and 3rd jet speeds, V_{j1} , V_{j2} , and V_{j3} , respectively, increase, while the experimental jet speeds decrease. Analytical and experimental results contradict each other. The similar trend exists in pressure results. Pressures increase at every step, while the measured pressures decrease at every step as shown in Table 2. This reflects the difference of 2nd and 3rd jet speeds

estimated from the pressures of 2nd (V_{j2}) and 3rd (V_{j3}) jet generation.

Table 1. Properties of fluid in each region of the x-t diagram

Region	P (Gpa)	ρ (kg/m3)	Up (m/s)	a (m/s)	C (m/s)	Vj (m/s)
1	0.0001	1000.00	0.00	1480.00	0.00	-
2	0.36	1115.31	192.91	1784.80	1865.82	-
3	1.05	1160.00	3.00	2340.47	1934.59	-
4	0.88	1189.00	375.00	2207.03	2250.00	1273.13
5	1.34	1206.57	97.90	2561.39	2536.28	-
6	1.80	1240.00	1.76	2902.12	2656.00	-
7	1.74	1265.00	228.00	2855.19	2800.00	1671.85
8	1.96	1257.80	42.27	3013.78	2986.66	-
9	2.33	1260.00	1.14	3269.69	3150.00	-
10	2.30	1301.00	144.00	3252.03	3190.00	1885.86

Table 2. Results for each experiment and their numerically estimated values.

Parameters	Pressure measurement inside the nozzle [23]	Visualization of high-speed liquid jet	1-D analysis of high- speed liquid jet
$\Delta t'_1$ (μ sec)	45.08	-	27.64
$\Delta t'_2$ (μ sec)	39.82	-	20.05
Δt_1 (μ sec)	-	32	37.41
Δt_2 (μ sec)	-	32	34.45
P_D (GPa)	1.24	-	0.88
P_E (GPa)	0.602	-	1.74
P_F (GPa)	0.273	-	2.3
V_{j1} (m/s)	-	1360 (max)	1273.13
V_{j2} (m/s)	-	495 (max)	1671.85
V_{j3} (m/s)	-	288 (max)	1885.86

It is concluded that the present analytical model should be modified. The wave reflection from an area convergence section and a straight nozzle is very different from that of the step shaped container. This trend is very well explained by the present sequential holographic interferometric visualization. In particular, at the later stage as seen in Fig. 8g-h, the mass flow thickens boundary layer displacement thickness along the nozzle wall and the container wall deformation would eventually reduce the jet speed. These effects have never been taken into account in this analysis. Lastly the presence of a diaphragm attached on the nozzle hole for preventing the liquid from dripping out of a nozzle, decisively governs the process of jet formation.

5. Conclusions

From the pressure history, sequential holographic interferograms inside the acrylic container and one-dimensional analysis, we found that: 1) longitudinal and transversal waves did exist in metal parts of the container and also in acrylic observation windows; 2) before the nozzle flow started, these waves and their reflected waves coalesced with a main impact generated shock wave; 3) the primary jet was driven by pressures of 12.4 GPa caused by 300 m/s projectile impingement; 4) successive shock reflections inside the container of liquid drove intermittent multiple liquid jets; 5) the contribution of released longitudinal and transversal waves to multiple jet formation is marginal; and 6) negative pressures detected with the optical fiber pressure transducer are attributable to impact flash and have no physical significance.

Acknowledgments

We wish to acknowledge Mr. S. Haysaka of Tohoku University for his encouragement and devotion in conducting the present experiments and all staff members of the Interdisciplinary Shock Wave Research Laboratory. We also wish to express gratitude to T. Kikuchi and D. Numata who helped in setting up the optical system. The first author would like to express his acknowledgement to Royal Thai Government for financial support. This project was in part supported by the Grant-in-Aid for Science Research No. 12 CE 2003 offered by the Ministry of Education, Culture, Sport, Science and Technology, Japan.

References

[1] Bowden, F.P., and Brunton, J.H., 1958. Damage to solids by liquid impact at supersonics speeds. *Nature*, Vol. 181, pp. 873-875.
 [2] Bowden, F.P., and Brunton, J.H., 1961. The deformation of solids by liquid impact at supersonic speeds. *Proc. Royal Society London*, Vol. 263 (series A), pp. 433-450.
 [3] Shi, H.H., 1994. Study of Hypersonic Liquid Jets. Ph.D. thesis, Tohoku University, Sendai, Japan, pp. 1-186.

[4] Shi, H.H., Takayama, K., and Nagayasu, N., 1995. The Measurement of impact pressure and solid surface response in liquid-solid impact up to hypersonic range. *Wear*, Vol. 186-187, pp. 352-359.
 [5] Obara, T., Bourne, N.K., and Field, J.E., 1995. Liquid-jet impact on liquid and solid surfaces. *Wear* Vol. 186-187, No. 2, pp. 388-394.
 [6] Pianthong, K., Zakrzewski, S., Behnia, M., and Milton, B.E., 2002. Supersonic Liquid Jets: their generation and shock wave characteristics. *Shock Waves*, Vol. 11, No. 6, pp. 457-466.
 [7] Shi, H.H., and Sato, H., 2003. Comparison-speed liquid jets. *Exp Fluids*, Vol. 35, pp. 486-492.
 [8] Pianthong, K., Milton, B.E., and Behnia, M., 2003. Generation and shock wave characteristics of unsteady pulsed supersonic liquid jets. *Atomization and Sprays*, Vol. 13, No. 5&6, pp. 475-498.
 [9] Bourne, N.K., 2005. On stress wave interactions in liquid impact. *Wear*, Vol. 258, pp. 588-595.
 [10] Pianthong, K., Takayama, K., Milton, B.E., and Behnia, M., 2005. Multiple pulsed hypersonic liquid diesel fuel jets driven by projectile impact. *Shock Waves*, Vol. 14, No. 1&2, pp. 73-82.
 [11] Pianthong, K., 2002. Supersonic liquid diesel fuel jets; generation, shock wave; Characteristics, Auto-ignition Feasibilities. Ph.D. Thesis, Univ New South Wales, Sydney, Australia, pp. 1-259.
 [12] O'Keefe, J.D., Wrinkle W.W., and Scully, C.N., 1967. Supersonic liquid jets. *Nature*, Vol. 213, pp. 23-25.
 [13] Ryhming, I.L., 1973. Analysis of unsteady incompressible jet nozzle flow. *J App Math & Phy (ZAMP)*, Vol. 24, pp. 149-164.
 [14] Glenn, L.A., 1975. The mechanics of the impulsive water cannon. *Comp & Fluids*, Vol. 3, pp. 197-215.
 [15] Lesser, M., 1995. Thirty years of liquid impact research: a tutorial review, *Wear*, Vol. 186-187, pp. 28-34.
 [16] Pianthong, K., Zakrzewski, S., Milton, B.E., and Behnia, M., 2003. Characteristics of impact driven supersonic liquid jets. *Exp Thermal and Fluid Sci*, Vol. 27, No. 5, pp. 589-598.
 [17] Milton, B.E., Watanabe, M., Saito, T., and Pianthong, K., 2005. Simulation of supersonic liquid jets using the Autodyne, *Proc 25th ISSW*, India, paper no.1185.
 [18] Ohashi, K., 2002. Experimental characterization of flow fields. Master Thesis, Graduate School of Tohoku University, Sendai, Japan, pp. 1-37.
 [19] Matthujak, A., Pianthong, K., Sun, M., Takayama, K., and Ikohagi, T., 2005. Characteristics of high-speed liquid fuel jets. 16th Japanese Symp Shock Wave, Yokohama, Japan, pp. 435-438.
 [20] Pecha, R.: Fiber optic probe hydrophone FOPH200: Technical description and instruction manual including service information, RP Acoustics, Germany, pp. 1-40.

- [21] Staudenraus, J., and Eisenmenger, W., 1993. Fiber-optic probe hydrophone for ultrasonic and shock-wave measurements in water. *Ultrasonic*, Vol. 31, No. 4, pp. 267-273.
- [22] Tepper, W., 1983. Experimental investigation of the propagation of shock waves in bubbly liquid-vapor-mixture, In: Archer, R.D., Milton, B.E.(eds) *Shock Tubes and Waves*, Proc 14th ISSW, pp. 397-404.
- [23] Matthujak, A., Hosseini, S.H.R., Takayama, K., Sun, M., and Voinovich, P. High speed jet formation by impact acceleration method. *Shock Waves Journal* (in press)